SAMES381

PERGAMON

Journal of South American Earth Sciences 00 (2002) 000–000

Journal of South American Earth Sciences

www.elsevier.com/locate/jsames

Petrology of spinel peridotite xenoliths from northeastern Brazil: lithosphere with a high geothermal gradient imparted by Fernando de Noronha plume

R.V. Fodor[a,*], A.N. Sial[b], G. Gandhok[a]

[a]*Department of Marine, Earth, and Atmospheric Sciences, College of Physical and Mathematical Sciences, North Carolina State University, Raleigh, NC 27695, USA*

[b]*Departamento de Geologia Universidade Federal de Pernambuco, Recife, PE, Brazil*

Received 1 September 2000; accepted 1 September 2001

Abstract

Spinel lherzolite, harzburgite, and clinopyroxenite xenoliths and pyroxene megacrysts in Tertiary alkalic basalts of northeastern Brazil (~30–13 Ma; K–Ar ages) provide information about melting, metasomatism, and geothermal gradients in subcontinental lithosphere as related to magmatism in that region since the Atlantic opening. That magmatism includes the xenoliths' host basalts, which have origins with the Fernando de Noronha plume, and regional tholeiitic basalts emplaced during continental rifting beginning ~200 Ma. Peridotite textures are largely protogranular, but some are porphyroclastic. Mineral compositions show correlations among Mg#s, Cr#s, and pyroxene Cr_2O_3, Al_2O_3, and Na_2O which suggest an upper-mantle history of varying melting and basalt extraction. Pyroxene equilibration temperatures range from ~800–1250 °C and represent a high geotherm, ~70–80 mW/m^2, or ~12 °C/km across the spinel stability field. Porphyroclastic xenoliths have the highest equilibration temperatures, >1150 °C. The equilibration temperatures do not correlate with the peridotite melting indicators (e.g. Cr#s; Cr_2O_3). In addition, Fe and Ti enrichments in minerals of porphyroclastic xenoliths, and light rare-earth element (LREE) enrichments, greatest in protogranular xenoliths (e.g. $La_{(n)}$ 2–16), each identify a metasomatic history for northeastern Brazil lithosphere.

Several of these xenolith features, particularly the geotherm they represent, can be linked to the Fernando de Noronha hotspot during Tertiary. The high geotherm likely originated as northeastern Brazil 'passed' over the plume. It was overprinted on subcontinental lithospheric mantle with existing melting characteristics that were possibly acquired during the earlier magmatism (e.g. Mesozoic) that attended the opening of the central Atlantic. The clinopyroxenite and the pyroxene megacrysts coexisting with the peridotite xenoliths likely represent Fernando de Noronha plume-derived basaltic melts that veined deformed lithosphere near plume margins to locally metasomatize that peridotite (porphyroclastic) with Fe and Ti. The LREE enrichments are probably also largely attributable to the plume, from which small percentage melts metasomatized the lithosphere to varying degrees, particularly the 'cooler', shallower level (protogranular) peridotite.

Keywords: Peridotite xenoliths; Brazil; Mantle composition; Mineral composition; Geotherm; Plume

1. Introduction

Spinel lherzolite and harzburgite xenoliths occur in seven Tertiary alkalic basalt centers of northeastern Brazil (Fig. 1). Fodor et al. (1998) described these basaltic centers and noted that they are of particular petrologic interest because their origins are likely tied to the Fernando de Noronha plume. Namely, South American plate movement during Tertiary placed northeastern Brazil in proximity of the Fernando de Noronha hotspot from about 35–15 Ma (Morgan, 1983; O'Connor and Duncan, 1990), which coincides with the K–Ar ages for the basaltic centers (Fodor et al., 1998). As described by Fodor et al. (1998), the alkalic basalts of northeastern Brazil largely represent asthenospheric melts from the plume that mixed with small amounts of lithospheric melts.

Given this tectonic and petrologic history, the peridotite xenoliths in the northeastern Brazil Tertiary lavas offer the opportunity to examine a portion of South American subcontinental lithosphere likely influenced by Fernando de Noronha plume. In addition, northeastern Brazil lithosphere experienced prior magmatism, namely Mesozoic dike-emplacement preceding and attending the central

* Corresponding author. Tel.: +1-919-515-3711; fax: +1-919-515-7802.
E-mail address: rfodor@ncsu.edu (R.V. Fodor).

0895-9811/02/$ - see front matter
PII: S0895-9811(02)00032-9

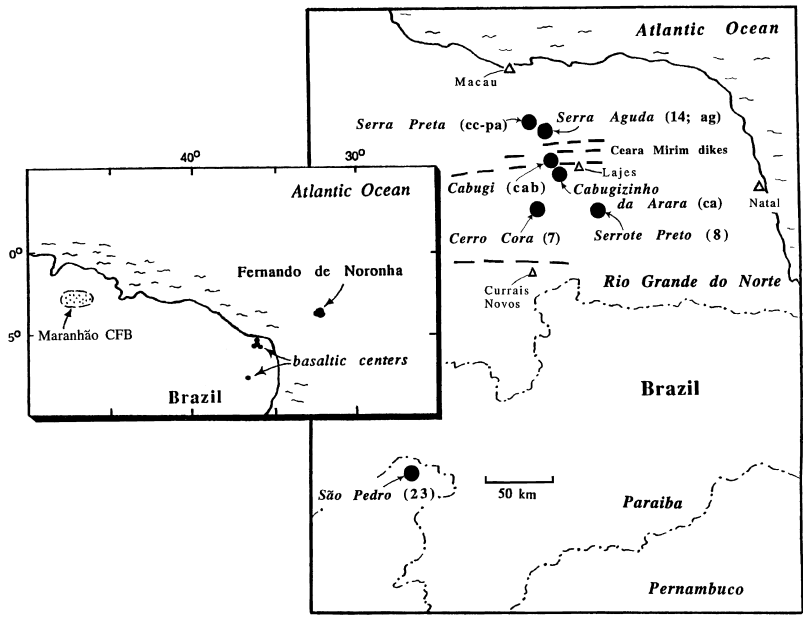

Fig. 1. Map showing locations and names of the seven Tertiary basaltic centers, northeastern Brazil, that yield peridotite xenoliths (sample codes in parentheses). Centers 'cab', '7', and '14' also yield clinopyroxenite xenoliths and pyroxene megacrysts. Included are locations of other northern Brazil Mesozoic basaltic magmatism: the Ceará–Mirim tholeiitic dikes (horizontal dashes; Bellieni et al., 1992), and the Maranhão flood basalts (inset; Fodor et al., 1990).

Atlantic breakup that led to the region becoming a passive margin. Both the Mesozoic and Cenozoic events potentially affected northeastern Brazil subcontinental lithosphere with elevated temperatures, partial melting, melt metasomatism, stress deformation, and re-equilibration of phase compositions or processes and features that may be manifested in xenolithic samples of subcontinental lithosphere.

Our approach to assessing this passive margin lithosphere through xenoliths was to examine 32 samples from the seven Tertiary alkalic basaltic centers for their petrography, mineral compositions, and, where samples were large enough, whole-rock compositions, including rare-earth elements (REE). We examine our data inclusive of previous studies (e.g. Rivalenti et al., 2000), but our emphasis for this xenolith- and basalt-rich province in northeastern Brazil is on how its lithosphere may manifest specific events related to the Fernando de Noronha plume and the earlier Atlantic opening. We also use a broad geographic coverage of sample sites and incorporate the pyroxene megacrysts and pyroxenite xenoliths that coexist with the peridotite xenoliths as part of the lithosphere's magmatic history. Most important all, however, mineral compositional data are of interest because they reveal a wide range in pyroxene equilibration temperatures (~450 °C). This equilibration temperature range, which is larger than that generally observed in xenolith provinces, is feasibly the signature of a high geothermal gradient imparted by a 'passing' asthenospheric plume.

2. Background

The seven northeastern Brazil alkalic basaltic centers are in Rio Grande do Norte, except for one in neighboring Pernambuco (Fig. 1). The peridotite xenoliths in some of these centers were first reported in Sial (1977), and some xenoliths were later included in a study by Comin-Chiaramonti et al. (1986). More recently, Princivalle et al. (1994) examined some xenoliths for pyroxene equilibration temperatures and pressures in view of xenolith textures. Also, Rivalenti et al. (2000) reported textures and clinopyroxene trace element and isotope compositions to create a model for metasomatism involving depleted lithospheric mantle infiltrated by fluids from enriched mantle components.

3. Petrography

The xenoliths at each site are small, generally 1–3 cm, but some reach 6–8 cm. Their abundances at the sites vary from sparse to relatively common. Three of the sites also have clinopyroxenite xenoliths, some up to ~6 cm, and cm-sized pyroxene megacrysts.

Most of the peridotites have protogranular textures, but four are porphyroclastic (Table 1). The protogranular textures have the characteristic (e.g. Mercier and Nicholas, 1975) curvilinear grain boundaries, grain sizes up to 5 mm, and rare kink banding in olivine. Additionally, a weak lineation overprints some protogranular samples. The

Table 1
Xenolith locations (see Fig. 1) listed as names for their Tertiary alkalic basaltic centers, northeastern Brazil, and respective sample numbers, peridotite types and textures, and equilibration temperatures (°C) (lherz = lherzolite; harz = harzburgite; harzburgite based on spinel Cr# >30, or, where spinel is absent in two xenoliths, harz based on clinoypyroxene Cr_2O_3 >1.2 wt%; proto = protogranular texture; porphyro = porphyroclastic texture; *T* (px-wells), pyroxene equilibration *T* after Wells (1977); *T* (px-bk), pyroxene equilibration *T* after Brey and Köhler (1990); *T* (ol-sp), olivine-spinel equlibration *T* after Ballhaus et al. (1991))

Location	Type	Texture	*T* (px-wells)	*T* (px-bk)	*T* (ol-sp)
Cerro Cora[a]					
7g	harz	proto	1090	1113	1149
7a	lherz	proto	970	1019	899
7d	lherz	proto	1196	1236	1195
Serrote Preto					
8d	lherz	porphyro	1171	1139	1144
8	lherz	proto	924	940	868
8a	lherz	proto	1082	1077	
8x	harz	proto	987	992	1095
8f	lherz	proto	1061	1054	1100
8v	lherz	proto	952	997	1011
Serra Aguda[a]					
14b	lherz	porphyro	1238	1254	1231
14e	lherz	proto	974	1013	861
ag2	lherz	proto	956	934	883
14a	lherz	proto	857	867	629
ag1	lherz	porphyro	1249	1275	1272
ag3	lherz	proto	967	1018	934
Sao Pedro					
23b	lherz	proto	950	940	
23c	lherz	proto	987	990	1069
23a	lherz	proto	996	1002	
Cabugi[a]					
cab1x	harz	porphyro	1248	1246	1407
Cab	lherz	proto	941	986	765
cab1	lherz	proto	1049	1097	1002
cab8	lherz	proto	1037	1112	901
cab3	lherz	proto	1072	1122	1065
Cabugizinha da Ara					
ca6	lherz	proto	993	1086	1121
ca4	harz	proto	943	952	
ca8	lherz	proto	985	1036	1086
ca1	lherz	proto	995	1038	820
Serra Preta					
cc-pa	lherz	proto	848	796	961
cc-pa3	lherz	proto	945	1002	824

[a] Clinopyroxenite xenoliths and pyroxene megacrysts are also present

porphyroclastic samples characteristically have large grains (>3 mm porphyroclasts) surrounded by fine mosaics of neoblasts, grain boundaries that are essentially straight, and conspicuous kink banding.

Reactions between host lavas and peridotites are generally limited to xenolith outer margins, but a few samples show that basaltic liquid has infiltrated fractures. Olivine and orthopyroxene grains within xenolith interiors appear to be pristine. In contrast, clinopyroxene grains, which are present in all samples, vary from having distinct contacts with neighboring olivine and orthopyroxene to having spongy rims that probably resulted from partial melting during ascent (e.g. Pike and Schwarzman, 1977). Also, some clinopyroxenes are spongy throughout and have become micromosaics of glassy blebs and clinopyroxene; original pyroxene in these 'relict' grains is difficult to locate for electron-beam analysis.

Spinel in xenoliths generally occurs as subrounded to anhedral, including hollyleaf-shaped grains, often associated with clinopyroxene. Some samples have intergranular relationships between pyroxene and spinel that might represent original presence of garnet (i.e. symplectites).

Because most xenoliths are small and our thin sections are on 2.5 cm slides (for microprobe analysis), the surface areas are unlikely to accurately represent modal mineralogy percentages (e.g. namely, from >1500 point counts). We accordingly classified the xenoliths as lherzolite and clinopyroxene-bearing harzburgite on the basis of spinel-Cr#s (atomic Cr/Cr + Al) where Cr# > 30 defines clinopyroxene-bearing harzburgite (e.g. Fan and Hooper, 1989; Batanova and Sobolev, 2000) (Table 1).

Evidence of reaction and resorption also surround the pyroxene megacrysts and the clinopyroxenite xenoliths, which have grains ≥1 cm. The products are mosaics of fine-grained olivine (≪ 0.1 mm) and interstitial glass.

4. Analytical techniques

We used an ARL-SEMQ electron microprobe at North Carolina State University (NCSU) to obtain mineral compositions. Reference minerals were olivine, pyroxenes, and spinel from the Smithsonian Institution as well as a Ni-doped diopside. Phi–rho–Z matrix corrections were used. For CaO in olivine, we used 20-s peak and background count times per spot, rather than the 'normal' 10-s times. Whole-xenolith major element compositions plus Ni were obtained by X-ray fluorescence spectrometry at NCSU. Rare-earth element abundances plus Sc were determined by neutron activation analyses at Oregon State University for certain xenoliths, for a clinopyroxene separate from one xenolith, and for a clinopyroxene megacryst. Before activation, samples were agitated in warm 10% HCl, soaked overnight, and washed in deionized water.

5. Mineral compositions

Average compositions for olivine, orthopyroxene, clinopyroxene, and spinel in peridotite xenoliths are in Tables 2–5. Abundances of the mineral major-elements Fe, Mg, Ca, and Al vary little within each xenolith, (standard deviations calculated for FeO, MgO, and CaO after 10–20 spot-analyses are listed in Tables 2–4). For example, FeO and MgO in olivine and orthopyroxene and CaO in clinopyroxene generally vary <2% of the amounts present. In contrast,

Table 2
Average olivine compositions for each peridotite xenolith (compositions are average values after 10–20 point analyses; s.d. = standard deviation)

	SiO_2	FeO	MnO	MgO	CaO	NiO	Total	Fo	FeO s.d.	MgO s.d.
Cerro Cora										
7g	40.9	8.5	0.13	50.7	0.12	0.47	100.82	91.4	0.14	0.40
7a	40.1	9.7	0.24	50.0	0.05	0.44	100.53	90.2	0.07	0.25
7d	39.8	8.7	0.08	50.6	0.12	0.44	99.74	91.2	0.14	0.27
Serrote Preto										
8d	39.6	13.0	0.07	46.8	0.11	0.38	99.96	86.5	0.13	0.22
8	39.9	8.7	0.19	49.9	0.03	0.46	99.18	91.1	0.16	0.23
8a	39.7	8.6	0.08	50.6	0.17	0.44	99.59	91.3	0.11	0.33
8x	40.3	8.3	0.11	51.5	0.04	0.43	100.68	91.7	0.14	0.40
8f	39.9	9.8	0.14	50.0	0.04	0.40	100.28	90.1	0.25	0.26
8v	40.0	9.0	0.13	51.0	0.05	0.45	100.63	91.1	0.11	0.40
Serra Aguda										
14b	39.1	11.1	0.17	48.3	0.15	0.36	99.18	88.6	0.30	0.36
14e	39.8	9.2	0.05	50.1	0.05	0.41	99.61	90.7	0.14	0.36
ag2	40.0	10.0	0.17	48.5	0.03	0.40	99.10	89.6	0.11	0.19
14a	41.0	9.7	0.18	48.9	0.05	0.44	100.27	90.0	0.17	0.38
ag1	40.2	8.9	0.12	51.1	0.17	0.41	100.90	91.1	0.06	0.23
ag3	40.2	9.3	0.16	49.3	0.04	0.43	99.43	90.4	0.10	0.37
Sao Pedro										
23b	40.0	8.8	0.13	50.1	0.04	0.46	99.53	91.0	0.14	0.34
23c	39.9	8.7	0.06	50.2	0.03	0.39	99.28	91.1	0.16	0.47
23a	40.2	9.4	0.14	50.6	0.04	0.39	100.77	90.6	0.12	0.30
Cabugi										
cab1x	40.2	9.2	0.15	50.6	0.17	0.44	100.76	90.8	0.21	0.33
Cab	39.8	9.3	0.12	50.2	0.03	0.42	99.87	90.6	0.12	0.24
cab1	39.9	8.7	0.16	49.8	0.08	0.41	99.05	91.1	0.10	0.38
cab8	40.7	9.9	0.16	49.1	0.07	0.43	100.36	89.8	0.09	0.32
cab3	40.0	9.1	0.14	50.8	0.07	0.43	100.54	90.9	0.11	0.27
C'zinha da Ara										
ca6	39.9	10.8	0.16	49.2	0.07	0.35	100.48	89.0	0.19	0.30
ca4	40.5	8.8	0.14	50.3	0.05	0.42	100.21	91.1	0.15	0.50
ca8	40.3	10.0	0.15	48.9	0.05	0.37	99.77	89.7	0.12	0.22
ca1	39.6	10.6	0.13	49.1	0.04	0.38	99.85	89.2	0.23	0.16
Serra Preta										
cc-pa	40.3	9.4	0.15	50.5	0.03	0.43	100.81	90.5	0.12	0.38
cc-pa3	40.3	9.3	0.14	49.9	0.06	0.40	100.10	90.5	0.10	0.29

CaO in olivine is slightly enriched near grain margins in more than half the xenoliths, and it varies from spot to spot by ~0.02 s.d. in some xenoliths that have olivine cores very low in CaO, <0.04 wt%. Average compositions for clinopyroxene and orthopyroxene as megacrysts and in a clinopyroxenite xenolith appear in Tables 3 and 4.

5.1. Xenoliths

5.1.1. Olivine and orthopyroxene

Nearly all xenoliths have olivine Fo and orthopyroxene Mg#s that are characteristic of mantle peridotite, between ~89 and 92, but two porphyroclastic xenoliths, 8d and 14b, are relatively Fe-enriched with olivine $Fo_{86.5}$ and $Fo_{88.6}$ and orthopyroxene Mg#s 86.6 and 88.5 (Fig. 2a). These two Fe-enriched porphyroclastic xenoliths a third, ag1 as well as have orthopyroxene enriched in TiO_2, 0.17–0.35 wt%, compared to <0.12 wt% in orthopyroxene of the other xenoliths (Fig. 2b).

Olivine Fo and orthopyroxene Mg#s correlate well across the xenolith suite (Fig. 2a), consistent with Fe–Mg exchange between these two minerals being virtually independent of temperature (Brey and Kohler, 1990). The suite also displays a wide range for CaO in olivine interiors, from 0.03 to 0.18 wt% (Fig. 2c). Comparing the CaO in olivine to the CaO in coexisting orthopyroxene (expressed as Wo end member) shows an overall positive relationship for the suite, but the correlation within small ranges of CaO is poor (Fig. 2c).

Among orthopyroxenes, there are wide variations in Al_2O_3 (2.6–6.7 wt%) and Cr_2O_3 (0.2–1 wt%), but no definable correlation between them (Fig. 2d). In contrast, orthopyroxene Cr_2O_3 and Mg# correlate positively, except for the highest Cr_2O_3 abundances (>0.6 wt%) and for the relatively Fe-enriched porphyroclastic xenoliths 8d and 14b (Fig. 2e).

Table 3
Average orthopyroxene compositions for each peridotite xenolith and one megacryst (compositions are average values after 10–20 point analyses; s.d. = standard deviation)

	SiO_2	TiO_2	Al_2O_3	Cr_2O_3	FeO	MnO	MgO	CaO	Na_2O	Total	Mg#	Fs	Wo	FeO s.d.	MgO s.d.
Xenoliths															
7g	53.9	0.03	3.6	0.77	5.6	0.12	33.1	1.1	0.13	98.35	91.3	8.5	2.1	0.08	0.24
7a	54.9	0.08	4.1	0.27	6.5	0.15	32.7	0.38	0.06	99.14	90.0	10.0	0.75	0.15	0.33
7d	54.3	0.07	5.4	0.83	5.5	0.12	32.2	1.35	0.13	99.90	91.3	8.5	2.7	0.08	0.18
8d	54.0	0.25	5.1	0.51	8.5	0.14	30.4	0.96	0.12	99.98	86.4	13.3	1.9	0.13	0.21
8	54.9	0.06	3.3	0.35	6.3	0.16	34.5	0.44	0.05	100.06	90.7	9.2	0.83	0.08	0.23
8a	53.5	0.10	6.1	0.90	5.6	0.14	31.6	1.3	0.16	99.40	91.0	8.8	2.6	0.10	0.27
8x	56.4	0.03	2.6	0.47	5.4	0.12	34.7	0.52	0.03	100.27	92.0	7.9	0.98	0.10	0.28
8f	55.6	0.08	4.0	0.29	6.5	0.14	32.7	0.42	0.06	99.79	90.0	9.9	0.82	0.11	0.42
8v	55.3	0.07	3.8	0.27	5.9	0.13	33.2	0.37	0.06	99.10	90.9	9.0	0.72	0.16	0.12
14b	52.5	0.35	6.7	0.63	7.1	0.14	30.0	1.5	0.13	99.05	88.3	11.4	3.1	0.08	0.11
14e	54.5	0.11	4.8	0.32	6.1	0.17	33.0	0.51	0.13	99.64	90.6	9.3	1.0	0.13	0.20
ag2	54.6	0.03	4.0	0.27	6.9	0.16	33.2	0.43	0.04	99.63	89.6	10.4	0.83	0.15	0.38
14a	54.5	0.09	3.7	0.21	7.2	0.15	33.0	0.44	0.08	99.37	89.1	10.8	0.85	0.11	0.12
ag1	53.5	0.17	6.1	0.94	5.7	0.12	31.7	1.6	0.18	100.01	90.8	8.9	3.2	0.12	0.44
ag3	54.9	0.09	3.7	0.22	6.2	0.15	34.5	0.40	0.04	100.20	90.8	9.1	0.75	0.12	0.30
23b	55.9	0.07	3.5	0.33	6.0	0.15	33.7	0.47	0.06	100.18	90.9	9.0	0.90	0.13	0.33
23c	55.8	0.08	3.4	0.48	6.1	0.15	34.0	0.39	0.05	100.45	90.9	9.1	0.74	0.17	0.39
23a	54.1	0.12	3.9	0.19	6.1	0.14	34.2	0.33	0.06	99.14	90.9	9.0	0.63	0.11	0.44
cab1x	53.9	0.06	4.6	1.05	5.9	0.11	31.9	1.7	0.02	99.24	90.6	9.1	3.4	0.10	0.21
Cab	53.5	0.09	4.5	0.39	6.1	0.14	35.0	0.47	0.08	100.27	91.1	8.8	0.87	0.09	0.45
cab1	55.3	0.04	3.7	0.50	5.7	0.12	33.0	0.67	0.08	99.11	91.2	8.7	1.3	0.07	0.39
cab8	53.7	0.06	5.4	0.29	6.3	0.14	32.8	0.71	0.12	99.52	90.3	9.6	1.4	0.10	0.29
cab3	54.0	0.06	4.8	0.51	5.9	0.12	32.8	0.85	0.12	99.16	90.8	9.0	1.7	0.10	0.23
ca6	54.1	0.05	4.7	0.30	6.8	0.14	32.8	0.58	0.19	99.66	89.6	10.3	1.13	0.14	0.20
ca4	55.0	0.07	2.6	0.54	5.8	0.13	35.7	0.61	0.12	100.57	91.6	8.3	1.11	0.12	0.26
ca8	54.7	0.11	4.4	0.31	6.4	0.14	33.2	0.56	0.10	99.92	90.2	9.7	1.08	0.12	0.35
ca1	54.3	0.10	4.3	0.23	6.9	0.14	32.9	0.54	0.09	99.50	89.5	10.4	1.05	0.11	0.34
cc-pa	55.0	0.09	3.9	0.34	6.0	0.13	33.4	0.43	0.11	99.40	90.8	9.1	0.83	0.14	0.37
cc-pa3	54.8	0.09	4.3	0.39	6.0	0.15	34.1	0.42	0.08	100.33	91.0	8.9	0.80	0.14	0.31
Megacryst															
14m	53.0	0.23	6.5	0.16	8.5	0.10	30.3	1.8	0.16	100.75	86.4	13.1	3.6		

5.1.2. Clinopyroxene

The Mg#s in clinopyroxene of most xenoliths are slightly higher than those in coexisting orthopyroxene (Fig. 3a), and their poor correlation reflects the dependency of Fe–Mg exchange on temperature (Brey and Kohler, 1990). There is, however, a well-defined inverse trend between CaO abundances in clinopyroxene and CaO in olivine (Fig. 3b), where porphyroclastic xenoliths have the lowest clinopyroxene Wo, (Fig. 2c shows the inverse relationship for orthopyroxene Wo). Within small ranges of CaO, however, the correlation is poor (Fig. 3b).

Clinopyroxene Cr_2O_3 and Al_2O_3 abundances vary widely among the xenoliths—from 0.3 to 1.8 wt% and from 1.4 to 8 wt%, respectively—and exhibit a general inverse correlation (Fig. 3c). In addition, Na_2O greatly varies (0.25–2.5 wt%) and the protogranular samples show good correlation with Al_2O_3 abundances (Fig. 3d). One REE pattern available for xenolithic clinopyroxene shows light-rare earth enrichment (Fig. 4a; Table 7).

5.1.3. Spinel

Throughout the xenolith suite, spinel Cr#s, in general, correlate positively with the Mg#s of coexisting olivine and orthopyroxene, except among Fe-enriched porphyroclastic xenoliths 8d and 14b and some xenoliths with low spinel Cr#s of ~8–12 (Fig. 5a). There is also an overall positive correlation for spinel Cr#s and Cr_2O_3 abundances in orthopyroxene and clinopyroxene (Figs. 5b and c). Among inverse correlations are those between spinel Cr#s and the Al_2O_3 abundances in both orthopyroxene and clinopyroxene (Fig. 5d and e) as well as between spinel Cr# and Na_2O in clinopyroxene (Fig. 5f). Finally, TiO_2 abundances in spinel are consistently low, <0.20 wt%, except for 0.46–1.04 wt% in porphyroclastic xenoliths 8d, 14b, and ag-1 (Fig. 5g).

5.2. Pyroxene megacrysts and clinopyroxenite

Clinopyroxene as megacrysts and comprising clinopyroxenite xenoliths is compositionally characteristic of the established variety of high Al_2O_3 clinopyroxene found in

Table 4
Average clinopyroxene compositions for each peridotite xenolith, two megacrysts, and one clinopyroxenite (compositions are average values after 10–20 point analyses; s.d. = standard deviation)

	SiO_2	TiO_2	Al_2O_3	Cr_2O_3	FeO	MnO	MgO	CaO	Na_2O	Total	Mg#	Fs	Wo	FeO s.d.	CaO s.d.	MgO s.d.
Xenoliths																
7g	53.7	0.13	2.3	1.8	2.6	0.08	17.6	20.4	0.63	99.24	92.3	4.3	43.5	0.08	0.12	0.29
7a	51.9	0.53	7.3	0.80	2.4	0.07	15.0	19.6	1.8	99.40	91.8	4.4	46.3	0.20	0.70	0.55
7d	52.1	0.27	6.3	1.3	3.3	0.10	18.2	17.6	1.1	100.27	90.8	5.7	38.7	0.07	0.12	0.13
8d	53.5	0.81	1.9	1.1	4.1	0.11	19.1	19.6	0.44	100.66	89.3	6.5	39.7	0.28	0.60	0.51
8	53.5	0.28	5.2	0.87	2.3	0.07	16.0	21.1	1.5	100.82	92.5	4.0	46.8	0.07	0.22	0.15
8a	52.9	0.63	2.9	1.3	3.2	0.09	18.0	21.3	0.47	100.79	90.9	5.1	43.6	0.30	0.36	0.54
8x	53.8	0.09	3.3	1.23	2.0	0.07	17.6	21.7	0.86	100.65	94.0	3.3	45.5	0.07	0.11	0.25
8f	52.6	0.32	4.2	0.98	2.5	0.05	18.0	21.3	0.51	100.46	92.8	4.0	44.1	0.11	0.27	0.26
8v	52.3	0.39	6.4	0.83	2.3	0.07	15.4	19.5	2.0	99.19	92.3	4.2	45.7	0.10	0.34	0.20
14b	49.9	0.80	8.1	0.88	4.6	0.12	18.0	16.0	1.04	99.44	87.5	8.0	35.9	0.11	0.24	0.18
14e	52.0	0.45	6.9	0.67	2.1	0.06	15.3	19.8	1.7	98.98	92.9	3.8	46.4	0.09	0.27	0.20
ag2	53.0	0.21	3.7	0.93	2.6	0.09	17.3	22.5	0.56	100.89	92.2	4.2	46.3	0.20	0.61	0.25
14a	52.1	0.61	7.0	0.64	2.2	0.09	14.1	20.5	1.9	99.14	92.0	4.1	49.0	0.09	0.23	0.11
ag1	51.5	0.37	7.2	1.4	3.5	0.10	18.7	16.4	1.1	100.27	90.5	6.0	36.4	0.11	0.43	0.73
ag3	52.3	0.49	6.6	0.63	2.1	0.05	15.4	19.8	1.7	99.07	92.9	3.8	46.2	0.15	0.51	0.62
23b	51.7	0.60	2.7	1.1	3.6	0.08	16.9	22.1	0.50	99.28	89.3	5.8	45.7	0.34	0.43	0.38
23c	53.2	0.27	3.9	1.4	2.3	0.07	17.0	21.6	0.85	100.59	92.9	3.8	45.9	0.21	0.53	0.70
23a	53.8	0.41	1.4	0.31	3.8	0.10	18.4	21.3	0.48	100.00	89.6	5.9	42.7	0.22	0.70	0.70
cab1x	52.1	0.13	4.8	1.2	3.5	0.10	19.4	18.2	0.24	99.67	90.8	5.7	38.0	0.05	0.17	0.20
Cab	52.6	0.43	6.7	0.90	2.3	0.07	15.5	20.4	1.7	100.60	92.3	4.1	46.6	0.10	0.18	0.19
cab1	53.2	0.17	5.1	0.99	2.7	0.09	16.7	19.7	1.3	99.95	91.7	4.7	43.8	0.04	0.15	0.21
cab8	52.8	0.34	7.3	0.54	3.1	0.08	15.3	18.9	1.7	100.06	89.8	5.7	44.4	0.11	0.15	0.12
cab3	53.0	0.14	5.9	0.97	2.9	0.08	16.9	19.5	1.3	100.69	91.2	5.0	43.1	0.10	0.11	0.18
ca6	53.1	0.36	8.0	0.72	3.1	0.08	14.8	18.1	2.5	100.76	89.5	5.9	44.1	0.11	0.17	0.25
c4	53.2	0.69	2.5	1.8	2.6	0.06	17.0	21.7	0.95	100.50	92.1	4.3	45.8	0.20	0.15	0.32
ca8	51.7	0.50	6.7	0.79	2.9	0.09	16.0	19.7	1.7	100.08	90.8	5.1	44.6	0.05	0.09	0.30
ca1	52.5	0.45	6.2	0.63	3.0	0.09	16.1	20.0	1.5	100.47	90.5	5.2	44.7	0.14	0.10	0.45
cc-pa	52.2	0.84	3.1	1.1	3.2	0.09	16.3	23.2	0.60	100.63	90.1	5.2	48.0	0.30	0.20	0.46
cc-pa3	53.0	0.45	7.0	0.84	2.5	0.08	15.2	19.7	2.1	100.87	91.6	4.6	46.1	0.10	0.29	0.29
Megacrysts																
7	49.7	0.86	8.5	0.03	6.8	0.12	16.4	16.8	1.3	100.51	81.1	11.8	37.4			
14g	51.7	0.44	7.4	0.39	5.6	0.16	18.9	15.6	1.0	101.19	85.7	9.4	33.7			
Clino'pxnt																
cab3	50.4	0.46	8.0	0.14	6.1	0.15	18.0	14.9	1.04	99.19	84.0	10.6	33.4			

continental alkalic basalts as grains and lithic fragments (e.g. Wilshire and Shervais, 1975; Righter and Carmichael, 1993). Those observed here are relatively evolved, Mg#s ~81–86. The REE abundances (Table 7) for one clinopyroxene megacryst (Fig. 4a; Table 7) exhibits a chondrite-normalized pattern that resembles those for clinopyroxene megacrysts in alkalic basalt lavas elsewhere (e.g. Irving and Frey, 1984; Shaw and Eyzaguirre, 2000).

The one orthopyroxene megacryst we analyzed is also of high Al and Ti variety and has an overall composition similar to orthopyroxene megacrysts in alkalic basalt lavas observed elsewhere (e.g. Irving and Frey, 1984). It is relatively evolved, Mg# ~86.

6. Geothermometry and geobarometry

We calculated xenolith equilibration temperatures (T_{eq}) from clinopyroxene and orthopyroxene compositions according to the two-pyroxene methods of Wells (1977) and Brey and Kohler (1990), and from olivine and spinel according to Ballhaus et al. (1991). Results from the two pyroxene methods correlate well over the large temperature range that the xenoliths yield, ~850 to ~1250 °C, Wells (1977), and ~800 to ~1250 °C Brey and Kohler (1990), as shown by the nearly linear relationship in Fig. 6a. Pyroxene in some Cabugi basaltic-center xenoliths reported by Rivalenti et al. (2000) extend the low end of the range to ~775 °C, using the Wells (1977) calibration (Fig. 6a).

The four porphyroclastic xenoliths have among the highest T_{eq} observed, ~1170–1250 °C (T_{Wells}), and all protogranular samples except one, 7d, have $T_{eq} < 1110$ °C (Fig. 6a). Notable, too, is that the entire T_{eq} range (including the samples of Rivalenti et al., 2000) is represented at a single center, Cabugi, and nearly the full T_{eq} range is observed in our Serra Aguda samples (Fig. 6b).

Table 5
Average spinel compositions for each peridotite (compositions are average values after 10–15 point analyses; Cr# = atomic Cr/(Cr + Al) × 100; Fe_2O_3 calculated stoichiometrically after determining all Fe as FeO)

	TiO_2	Al_2O_3	Cr_2O_3	FeO	Fe_2O_3	MnO	MgO	Total	Mg#	Cr#
7g	0.12	34.0	33.3	11.0	3.2	0.16	17.6	99.38	74.0	39.7
7a	0.07	60.4	7.8	9.1	0.82	0.10	21.2	99.49	80.6	8.0
7d	0.25	46.8	20.8	9.6	2.8	0.11	20.0	100.36	78.8	23.0
8d	1.04	47.0	15.7	13.5	4.6	0.10	17.4	99.34	69.7	18.3
8	0.07	52.0	15.5	10.1	1.3	0.11	19.6	98.68	77.6	16.7
8x	0.14	36.0	33.4	10.6	2.3	0.16	18.2	100.80	75.4	38.4
8f	0.15	59.0	9.3	9.3	1.9	0.07	21.5	101.22	80.5	9.6
8v	0.07	57.1	11.8	9.0	1.5	0.13	21.3	100.90	80.8	12.2
14b	0.68	53.3	12.0	10.8	3.5	0.09	19.9	100.27	76.7	13.1
14e	0.04	61.3	7.8	9.2	0.82	0.11	21.5	100.77	80.7	7.9
ag2	0.01	58.1	10.9	10.1	1.0	0.12	20.6	100.82	78.4	11.2
14a	0.04	61.4	7.5	10.9	0.23	0.09	20.2	100.36	76.8	7.6
ag1	0.46	46.6	21.3	9.4	3.0	0.12	20.2	101.08	79.3	23.5
ag3	0.04	59.4	7.8	8.8	0.96	0.11	21.0	98.11	81.0	8.1
23c	0.14	48.6	19.8	9.3	1.7	0.15	20.0	99.69	79.3	21.5
cab1x	0.24	34.5	31.7	9.9	3.9	0.13	18.4	98.77	76.8	38.1
Cab	0.09	57.5	11.9	10.3	0.7	0.12	20.4	101.01	77.9	12.2
cab1	0.16	45.2	22.3	10.5	2.1	0.13	18.9	99.29	76.2	24.9
cab8	0.09	60.9	7.4	10.0	1.3	0.12	21.0	100.81	78.9	7.5
cab3	0.09	49.3	17.6	9.8	2.2	0.11	19.7	98.80	78.2	19.3
ca6	0.12	56.4	9.4	10.0	2.4	0.12	20.3	98.74	78.4	10.1
ca8	0.15	56.6	11.3	9.8	2.0	0.11	20.8	100.76	79.1	11.8
ca1	0.11	58.0	9.5	11.8	1.7	0.13	19.6	100.84	74.7	9.9
cc-pa	0.04	55.8	11.9	9.6	1.5	0.15	20.5	99.49	79.2	12.5
cc-pa3	0.06	56.7	11.6	10.1	1.0	0.13	20.2	99.75	78.1	12.1

The olivine-spinel equilibration temperatures only generally correlate with those derived from the pyroxene calibrations, mainly underestimating the low pyroxene temperatures and overestimating the mid-range pyroxene temperatures. (Fig. 6c). They nonetheless confirm the large equilibration temperature range of the xenolith suite that pyroxene geothermometry manifests.

For geobarometry, we applied the Ca-olivine/Ca-clinopyroxene method of Köhler and Brey (1990), which is based on CaO in olivine decreasing with pressure and increasing with temperature. The wide range in olivine-CaO in our xenolith suite shows the positive relationship between CaO and temperature (Fig. 7a) as is expected as determined from experiments (e.g. Köhler and Brey, 1990). But it shows a poor relationship for pressure, where high CaO is expected (from experiments) to associate with low *P* (Fig. 7b). The calculated pressure range exceeds that for the spinel-peridotite stability field, both over- and under-estimating its ~10–22 kbar range for spinel stability (e.g. Webb and Wood, 1986) (Fig. 7c). The inability to construct a meaningful *P–T* relationship for the entire xenolith using Ca-olivine/Ca-clinopyroxene is not surprising, however, due largely to the difficulty in accurately analyzing low Ca concentrations (e.g. <0.05 wt% CaO; O'Reilly et al., 1997). There is also a problem due to absence of Ca equilibrium between olivine and clinopyroxene (e.g. Fig. 3b) because Ca diffuses more readily in olivine than in clinopyroxene (e.g. Köhler and Brey, 1990).

7. Whole-xenolith compositions

Of the ten xenoliths analyzed, seven are protogranular and three are porphyroclastic. Compositions appear in Tables 6 and 7 and in MgO variation diagrams of Fig. 8. To express how the xenoliths compare to peridotite xenoliths elsewhere, Fig. 8 includes the compositional fields for a lherzolite–harzburgite suite from French Massif Central. Correlations among the northeastern Brazil xenoliths include the generally increasing SiO_2, TiO_2, Al_2O_3, and CaO abundances with decreasing MgO, and an essentially flat trend for K_2O and FeO relative to MgO. Sample 8d, an exception, displays comparatively low SiO_2, Al_2O_3, and CaO, and high K_2O and FeO (Fig. 8a–f). CaO and Al_2O_3, both relatively easily removed during partial melting of peridotite, weakly covary over a relatively wide compositional range (Fig. 8g).

REE abundances in nine xenoliths are listed in Table 7. REE patterns in Fig. 4b–d show that all have at least some LREE enrichment, and that nearly all patterns are flat in the middle to heavy REE segments. The LREE enrichments vary. Among protogranular xenoliths, chondrite-normalized

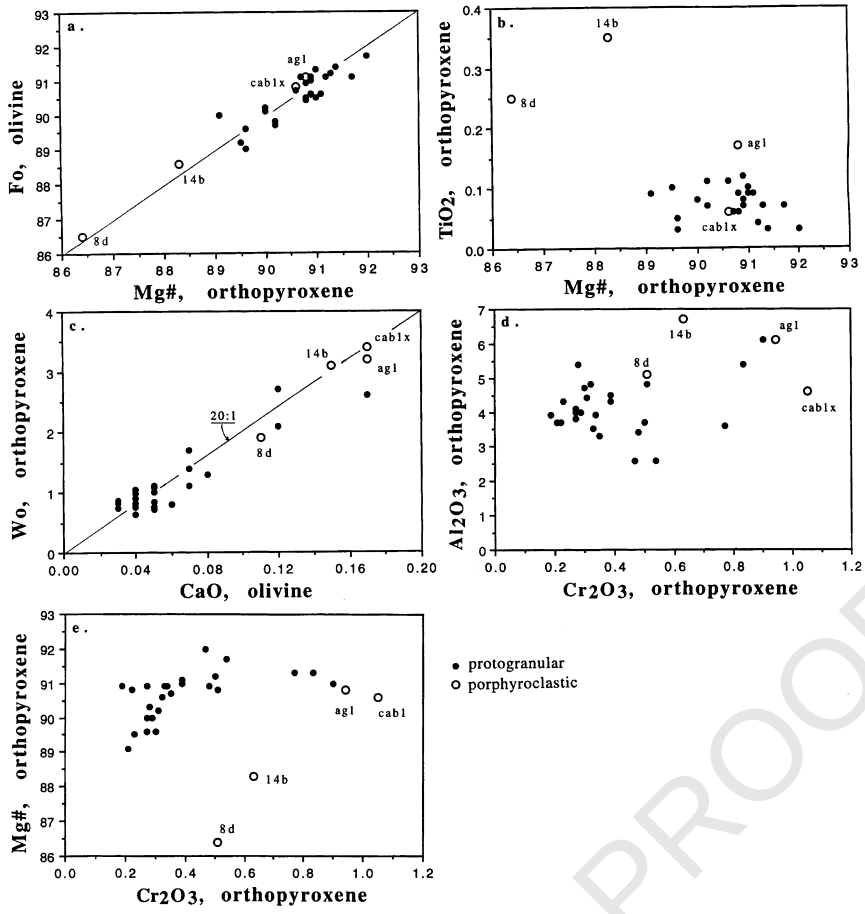

Fig. 2. Variation diagrams for average compositions of olivine and orthopyroxene in peridotite xenoliths of Tertiary alkalic basalts, northeastern Brazil, expressed as two textural types, protogranular and porphyroclastic. Note the relative Fe and Ti enrichment of two porphyroclastic xenoliths, 14b and 8d, and the wide range of CaO in olivines. Sample numbers identify the data points for porphyroclastic xenoliths (see Fig. 1, Table 1).

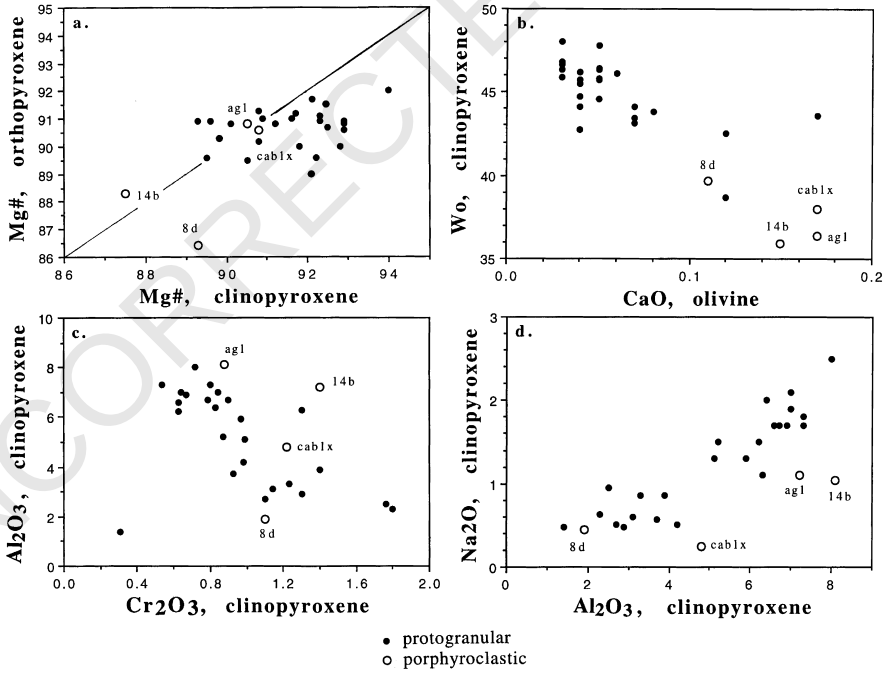

Fig. 3. Various aspects of clinopyroxene average compositions in the peridotite xenoliths, northeastern Brazil. Panel b shows a general correlation for CaO in olivine and clinopyroxene but no detailed correlation, which is relevant for estimating thermobarometry.

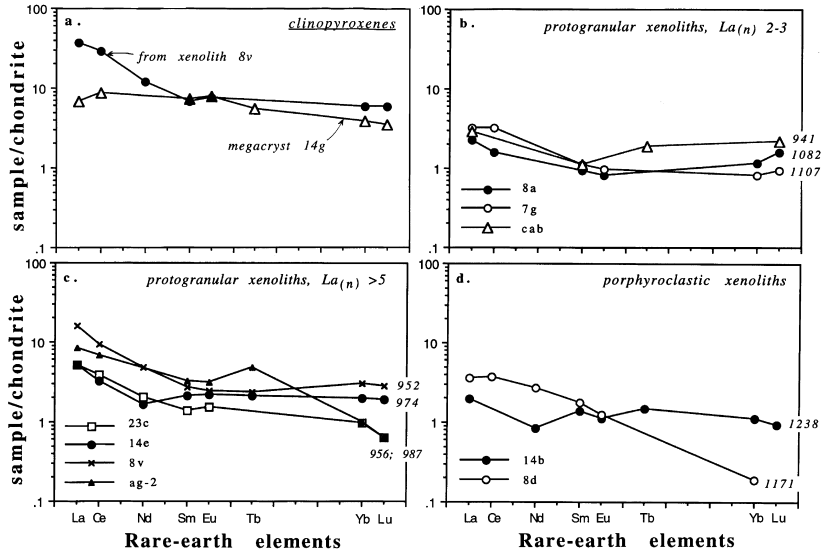

Fig. 4. Rare-earth element patterns, ordinary-chondrite normalized. (a) Patterns for a clinopyroxene megacryst (14g) in a lava at Serra Aguda basaltic center and for clinopyroxene separated from a lherzolite xenolith at Serrote Preto (8) (see Fig. 1, Table 1). (b–d) Whole-xenolith patterns, arranged in two groups of La for protogranular. Numbers at ends of patterns are pyroxene equilibration temperatures, °C, after Wells (1977) (see Table 1).

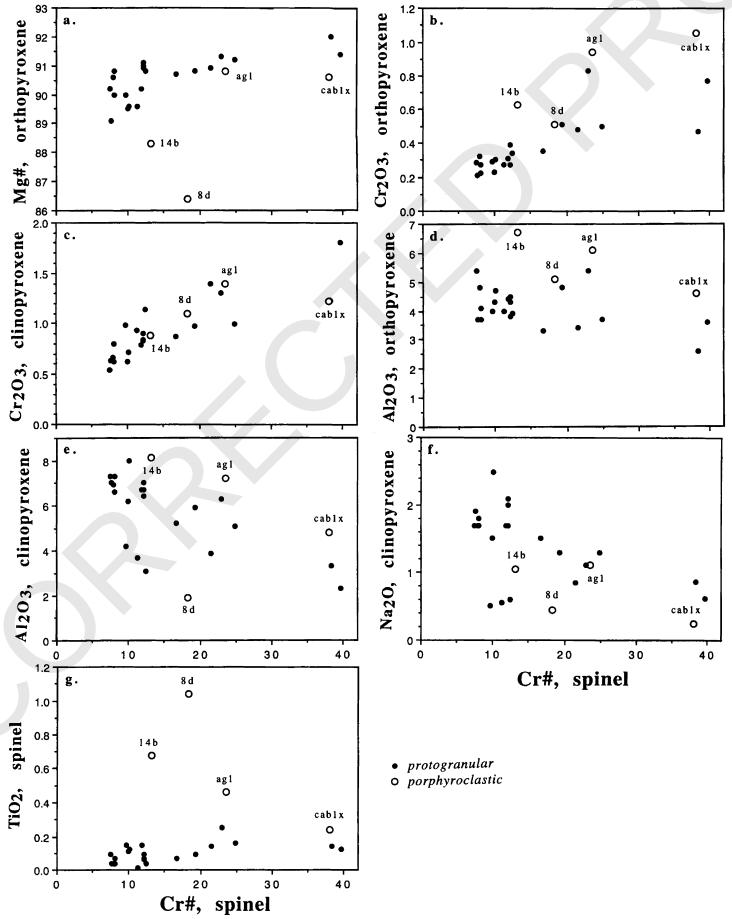

Fig. 5. Variation diagrams based on average Cr#s (atomic Cr/Cr + Al × 100) for spinel in the peridotite xenoliths, largely illustrating how spinel compositions covary with those of coexisting silicate minerals (a–f) as well as the relative Ti-enrichment of spinel in porphyroclastic xenoliths 14b and 8d (panel g).

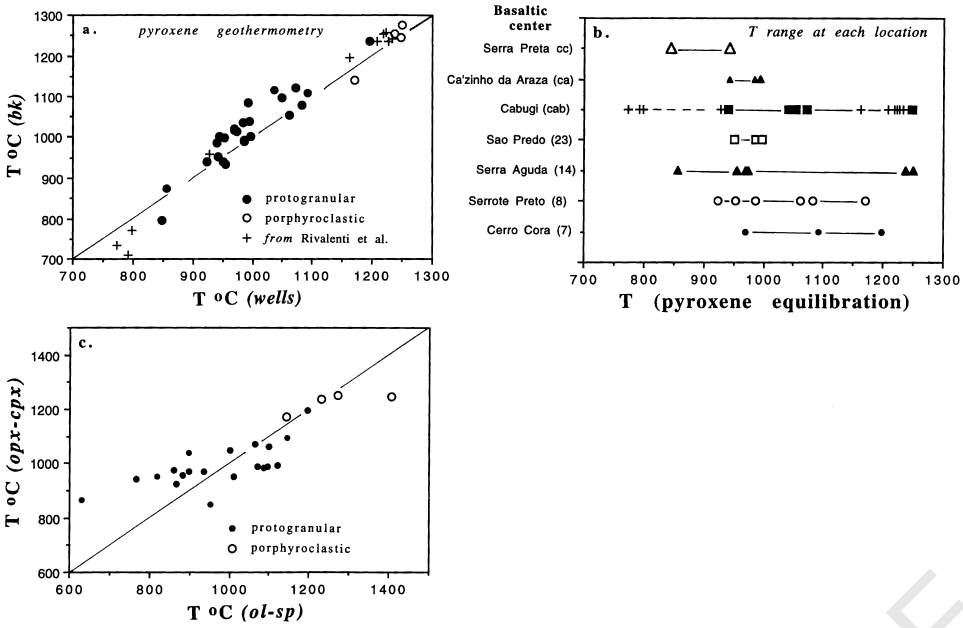

Fig. 6. (a) Comparison of pyroxene equilibration temperatures for xenoliths based on Wells (1977) and Brey and Kohler (1990) (T °C bk). (b) The ranges of pyroxene equilibration temperatures (after Wells, 1977) observed among xenoliths from each of the seven basaltic centers in northeastern Brazil (see Fig. 1). Cabugi line includes data from Rivalenti et al. (2000) at + symbols. (c) Comparison of olivine-spinel equilibration temperatures (Ballhaus et al., 1991) to pyroxene temperatures (after Wells, 1977).

La ranges from ~2 to 16 (Fig. 4b and c), but all are essentially more enriched in LREE than the two porphyroclastic xenoliths analyzed (Fig. 4d). The most LREE-enriched protogranular samples have among the lowest T_{eq} (Fig. 4b and c). The same enrichment relationship between protogranular and porphyroclastic xenoliths was observed by Rivalenti et al. (2000) for their xenoliths from Cabugi basaltic center in this region. In contrast, some xenolith suites from other regions have porphyroclastic xenoliths with greater LREE enrichment than protogranular xenoliths (e.g. Downes, 1990; Bedini et al., 1997).

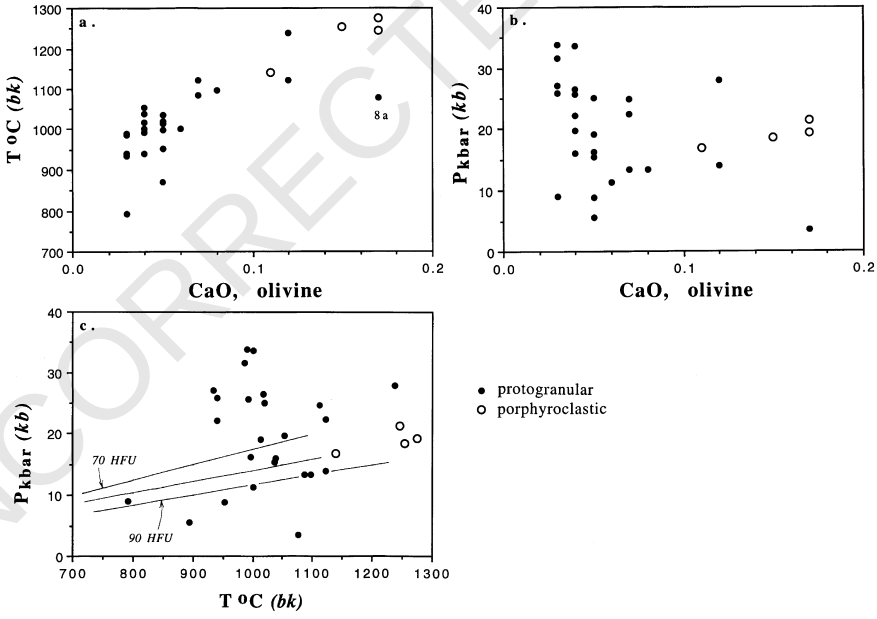

Fig. 7. (a) The general correlation between pyroxene equilibration temperatures for xenoliths calculated according to Brey and Kohler (1990) (T °C bk) and CaO in olivine. (b, c) The poor relationship between pressure (kbar) calculated according to Kölher and Brey (1990) (P kb) and CaO in olivine and pyroxene equilibration temperatures (after Brey and Kohler, 1990), probably due to lack of Ca equilibration between coexisting clinopyroxene and olivine in the xenoliths (see Fig. 3b). Geotherms are based on Chapman (1986).

Table 6
Whole-xenolith compositions (in wt% and ppm) of spinel lherzolite and spinel harzburgite, Tertiary alkalic basalt centers, northeastern Brazil

	SiO_2	TiO_2	Al_2O_3	FeO[a]	MnO	MgO	CaO	Na_2O	K_2O	P_2O_5	Total	Mg#	Ni	Cr
8d	42.60	0.22	2.27	14.57	0.15	39.55	1.04	0.22	0.16	0.02	100.80	82.9	2050	2730
8a	43.71	0.13	2.41	8.92	0.14	43.05	1.86	0.41	0.01	0.02	100.66	89.6	2305	2870
8f	44.09	0.13	2.96	8.71	0.14	40.93	3.14	0.41	0.04	0.05	100.60	89.3	2185	1975
8v	44.03	0.16	3.10	8.22	0.14	41.91	2.51	0.52	0.09	0.06	100.74	90.1	2415	2645
14b	44.12	0.19	2.70	9.93	0.14	41.35	2.25	0.13	0.01	0.01	100.83	88.1	2220	2090
14e	44.62	0.19	5.10	8.09	0.14	38.20	4.31	0.29	0.01	0.03	100.98	89.4	2020	2725
ag2	43.16	0.09	2.37	8.93	0.14	42.03	3.79	0.39	0.03	0.04	100.97	89.4	2345	1810
ag1	43.33	0.09	1.72	8.03	0.13	45.52	1.69	0.14	0.01	0.01	100.67	91.0	2405	2405
cab	43.35	0.06	1.83	8.87	0.14	45.31	0.94	0.14	0.01	0.03	100.68	90.1	2775	1300
cab3	44.04	0.07	2.92	8.07	0.13	43.02	2.31	0.23	0.01	0.09	100.89	90.5	2305	3100

[a] All Fe as FeO.

8. Discussion

8.1. Melting and equilibration temperature histories

Some of the compositional relationships among the minerals comprising the xenoliths as well as some between minerals and whole-xenoliths indicate that the peridotite suite represents mantle that underwent varying degrees of melting and basalt extraction. Such relationships were first observed for northeastern Brazil xenoliths by Comin-Chiaramonti et al. (1986) and, as shown in Fig. 5, include the general increasing of spinel Cr#s with increasing silicate-phase Mg#s and Cr_2O_3 abundances and decreasing clinopyroxene Al_2O_3 and Na_2O. Other examples of histories of varying melting include the ranges for and the correlations between Al_2O_3 and Na_2O in clinopyroxene and Al_2O_3 and CaO among whole-xenolith compositions (Figs. 3d and 8g).

However, there is lack of correlation between the equilibration temperatures (ranging from ~825 to 1250 °C; Fig. 6a) and melting history indicators, such as Mg#s, Cr#s, and Cr_2O_3, Al_2O_3, and Na_2O abundances in minerals (Fig. 9a–d). The melting histories recorded in the xenoliths thus, reflect processes that occurred in subcontinental lithosphere before the thermal event(s) responsible for the wide range in T_{eq}. They are not related to the formation of the Tertiary basaltic magmas that entrained these xenolithic representations of the lithosphere and 'captured' their equilibration temperatures.

Because all xenoliths are spinel peridotite, and because one of our objectives is to evaluate the geotherm present at Tertiary magmatism, we can estimate a minimum gradient by first assigning the large T_{eq} range as an overprint on the entire spinel peridotite stability field of subcontinental lithosphere at the time of Tertiary basalt eruption. Access to the xenoliths' full T_{eq} range (Fig. 6b) at single vents (e.g. Cabugi) is consistent with viewing the T_{eq} range as a gradient across the spinel peridotite vertical interval. There is no reliable method for determining equilibration pressures for spinel peridotite, however, and we therefore, cannot quantitatively constrain the pressures represented by each T_{eq}.

Table 7
Trace-element abundances (in ppm) in peridotit exenoliths, in clinopyroxene from a xenolith, an din a clinopyroxene megacryst

	La	Ce	Nd	Sm	Eu	Tb	Yb	Lu	Sc	Hf	Th
Xenolith											
7g	1.0	2.6		0.22	0.07		0.17	0.03	9.0	0.23	0.09
8d	1.1	3.0	1.6	0.34	0.09		0.04		6.5	0.3	
8a	0.7	1.3		0.18	0.06		0.24	0.05	10.0	0.2	0.1
8v	5.0	7.6	2.9	0.53	0.18	0.11	0.62	0.09	11.9		1.5
14b	0.6	0.2	0.5	0.27	0.08	0.07	0.23	0.03	7.9	0.3	0.9
14e	1.6	2.6	1.0	0.41	0.16	0.10	0.41	0.06	14.8	0.35	1.1
ag2	2.6	5.5		0.62	0.23	0.11	0.21	0.03	9.0	0.4	0.5
23c	1.6	3.1	1.2	0.27	0.11		0.20	0.02	6.1	0.21	0.6
Cab	0.9			0.22	0.042	0.09		0.07	6.1	0.18	
Clinopyroxene megacryst											
14g	2.10	6.9		1.43	0.56	0.26	0.81	0.11	40.4	1.10	
Clinopyroxene, xenolith 8											
8v	11.3	23.4	7.2	1.30	0.55		1.25	0.19	57.4	1.30	
Uncertainty %	3	7	12	5	5	5	5	5	3	5	5

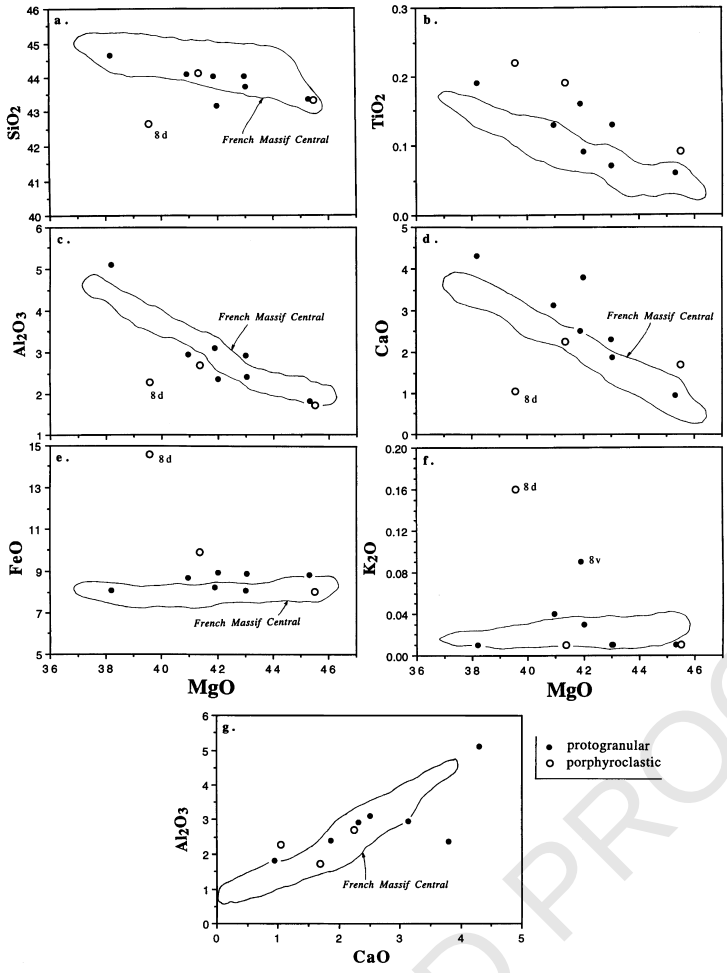

Fig. 8. Whole-rock compositions for 10 xenoliths compared with compositional fields for a comprehensive peridotite suite from French Massif Central (Zangana et al., 1997). Note that porphyroclastic xenolith 8d largely stands apart by its relative enrichments (e.g. Fe, K) and depletions (e.g. Si, Al).

We can, however, in the fashion of O'Reilly and Griffin (1996) and Xu et al. (1996), assign the lowest T_{eq} observed as representing the uppermost zone of spinel peridotite stabililty, or the maximum depth of the crust–mantle boundary. A reasonable approximation of this temperature is about 800 °C (Fig. 6a). On the basis of gravity and isostasy studies by Castro et al. (1997a,b)), which show Rio Grande do Norte crust to be ~30 km thick, we can estimate the ~800 °C T_{eq} as representing ~9 kbar pressure.

In the absence of garnet peridotite, we assign the high end of the T_{eq} range, ~1250 °C, to represent the maximum depth for the transition of spinel peridotite to garnet peridotite stability. Experimental determinations for the spinel garnet phase boundary show that this is ~20–22 kbar pressure, or approximately 65 km depth (e.g. O'Neill, 1981; Webb and Wood, 1986; Klemme and O'Neill, 2000). Combining the ~65 km depth for high T_{eq} xenoliths with the ~30 km depth for low T_{eq} xenoliths yields a minimum temperature gradient for the conductive lithosphere at the time of Tertiary basalt eruptions. That is, when considering that spinel peridotite is stable throughout an approximately 35 km zone of upper mantle, the constructed geotherm is ~12 °C/km. This equates to about 70–80 mW/m^2, which is notably higher than geotherms observed for continental shields and stable continents (nonrifting), which generally manifest heat flows of <50 mW/m^2 (e.g. Chapman, 1986).

One caution regarding this procedure for geotherm estimation comes from Xu et al. (1998), who point out that a portion of the Rhonda peridotite massif manifests essentially juxtaposed layers of low and high temperatures of equilibrations. That chance situation is probably attributable to a combination of relative diffusion rates, porosity, and locations with respect to infiltration and recrystallization fronts in the massif.

Both the melting and the T_{eq} histories of the xenoliths should be evaluated in terms of the two magmatic events that involved northeastern Brazil subcontinental lithosphere since the long continental stability beginning ~350–400 Ma, after Brazil was joined to the African continent in the region of the Benue trough (e.g. Affaton et al., 1991; Dallmeyer and Lecorche, 1991; Darros de Matos, 1992). One event was Mesozoic magmatism that accompanied the opening of the north and equatorial Atlantic regions beginning ~200 Ma and extended across large portions of

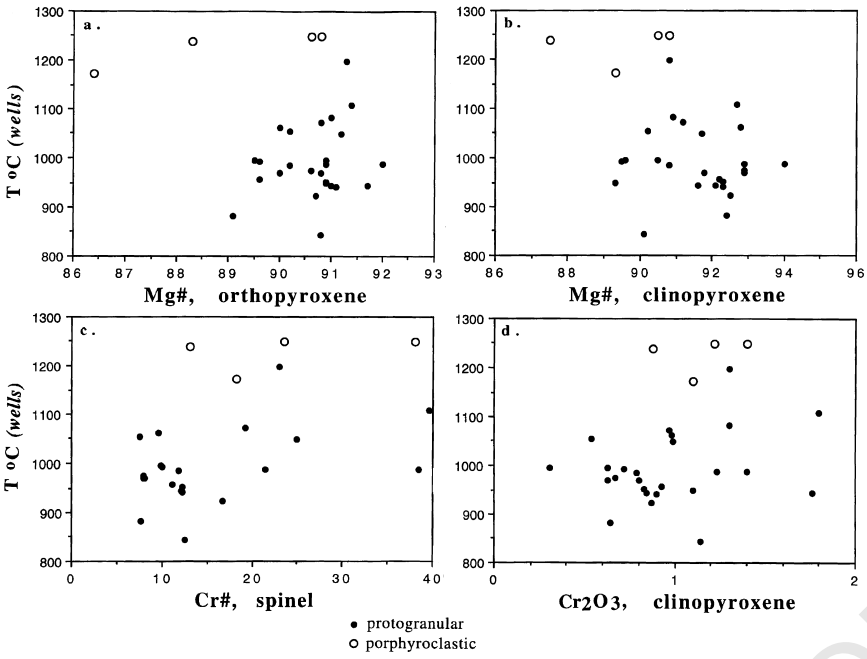

Fig. 9. Variation diagrams to illustrate how pyroxene equilibration temperatures (after Wells, 1977) do not correlate with the whole-rock compositional indicators of melting and basalt extraction, namely Cr and Mg abundances. This suggests that the events causing xenolith mineral equilibrations occurred independent of the partial melting events.

northern Brazil (e.g. Fodor et al., 1990; Wilson, 1997; Leitch et al., 1998; Marzoli et al., 1999). A component of that Mesozoic magmatism identified as the Ceará–Mirim tholeiitic basalt dike swarm (Bellieni et al., 1992) overlaps some of the sites for the spinel peridotite xenoliths (Fig. 1). The Ceará–Mirim dikes have K–Ar ages of ~175–130 Ma (Bellieni et al., 1992). Their emplacement, therefore, occurred long after stabilization of Gondwanaland, but long before equatorial separation of South America from Africa at ~115 Ma (e.g. Rabinowitz and LaBreque, 1979; Nurnberg and Muller, 1991) and the Tertiary alkalic basalts (30–13 Ma). But because subcontinental lithosphere was the source for this Mesozoic event (Bellieni et al., 1992), the melting that yielded the Ceará–Mirim dikes feasibly created some of the xenolith compositional characteristics that depict melt histories (Figs. 2,3,5 and 8). This is not to discount, however, compositional effects created by any late Proterozoic melting events in the lithosphere now underlying northeastern Brazil.

More relevant is that Ceará–Mirim dikes identify a magmatic event that could have elevated the northeastern Brazil geotherm prior to the Tertiary magmatism that incorporated the xenoliths. But any thermal effects of this Mesozoic magmatism on rifted and stretched lithosphere that long had been stable Gondwanaland lithosphere would have dissipated by inception of the Tertiary alkalic basalt magmatism in Rio Grande do Norte. This assessment holds despite the low thermal conductivity and diffusity of geologic material. For example, a calculation using thermal diffusivity of 10^{-6} m^2/s indicates that dissipation of geothermal perturbation across 50 km of upper mantle (a thickness greater than the spinel peridotite regime) would have occurred within ~80 My The xenolith-based geotherm is, therefore, unlikely to be a remnant from thermal perturbations during the continental breakup of the central Atlantic region.

Alternatively, and more likely, the relatively high geotherm of 70–80 mW/m^2, or that yielding ~1250 °C at ~20–22 kbar, represents thermal perturbation from the second magmatic event, namely, impingement of the Fernando de Noronha plume on northeastern Brazil subcontinental lithosphere beginning ~40 My. Elevated temperatures could have reached ~1300 °C and been recorded by coexisting pyroxenes in portions of the mantle currently represented as the xenoliths erupted beginning ~30 Ma.

Partial melting of the plume provided the bulk of the basaltic magmas that entrained the xenolith suite of lithosphere samples that bore the plume-related geotherm ~30–13 Ma (Fodor et al., 1998). The plume could also have served as the mechanism for creating porphyroclastic textures and the source for the REE and Fe–Ti enrichment processes indicated (Figs. 2a,b and 5g), as is discussed next.

8.2. Texture and T_{eq}

The high T_{eq} observed among porphyroclastic xenoliths suggests that these upper mantle samples were in regimes of both elevated temperatures and shear deformation. The margins of an ascending plume provide such an environment for this correlation, where significantly higher temperatures are not only expected, but also the dynamics necessary to create porphyroclastic textures (e.g. Witt and

Seck, 1987; Downes, 1990). Whereas the porphyroclastic xenoliths all have >1150 °C T_{eq}, protogranular xenolith 7d also has notably high T_{eq}, ~1190 °C (Table 1), suggesting that there is not an exclusive relationship between high, plume-induced temperatures and the development of strained textures.

8.3. Metasomatic enrichments

Fig. 4 shows that the xenoliths have varying amounts of LREE enrichments, in spite of whole-rock and mineral compositions that indicate melting histories that removed basaltic components (Fig. 8). Such LREE enrichments observed in mantle xenoliths and their clinopyroxenes (Fig. 4a–c) are generally attributed to metasomatic fluids chromatographically percolated through upper mantle peridotite previously depleted in incompatible elements (e.g. Navon and Stolper, 1987; Song and Frey, 1989; Franz et al., 1997; Zangana et al., 1997, 1999). In this case, the source of the fluids is feasibly the asthenospheric melting associated with the Fernando do Noronha plume. Additional expressions of metasomatism in the northeastern Brazil xenoliths are presented as clinopyroxene trace-element compositions by Rivalenti et al. (2000) and in Fig. 4a, as clinopyroxene Sr–Nd isotope compositions in Rivalenti et al. (2000), and as a clinopyroxene Sr–Nd–Pb isotope composition in Fodor et al. (1998).

According to the T_{eq} associated with each REE pattern (Fig. 4b–d), lithospheric mantle represented by the mid- to low-temperature portions of the gradient and with protogranular texture was more enriched in LREE than was high-temperature, porphyroclastic-textured mantle. This relationship is likely a result of porous melt flow, the effects of which and the modeling for which are variable and complex (e.g. Godard et al., 1995; Vernieres et al., 1997; Bedini et al., 1997). The most straightforward explanation for our observations is that the high-temperature porphyroclastic xenoliths were relatively close to the source of the metasomatizing fluids (e.g. ocean island basalt composition; Fodor et al., 1998) and had porosity to provide relatively high melt/rock ratios for high melt fractions. This situation can yield metasomatic characteristics with nominal to flat LREE/HREE ratios (Bedini et al., 1997). In contrast, the lower-temperature protogranular xenoliths represent relatively low porosity (and therefore, low melt/rock ratio) peridotite located relatively far from the source for metasomatizing fluids. Characteristics of those infiltrating plume-derived fluids would be high LREE/HREE ratios due to progressive melt-rock reactions and decreasing melt mass coupled with chromatographic effects during upward migration (Bedini et al., 1997).

Rivalenti et al. (2000) first observed these textural and REE correlations in their collection of xenoliths from Cabugi basaltic center. Here we add to the metasomatic history of the porphyroclastic xenoliths to support their metasomatism by basalt composition melts. Namely, we observe that in addition to having higher T_{eq}, a deformed textural type due to plume proximity, and lower LREE enrichments than protogranular xenoliths (Fig. 4), two porphyroclastic xenoliths (8d and 14b) have relatively low Mg#s in olivine and pyroxene and high TiO_2 in orthopyroxene and spinel (Figs. 2a,b and 5g). Such Fe and Ti enrichment (e.g. Harte, 1987; Bodinier et al., 1990; Witt-Eickschen et al., 1993) is a feature often associated with deformed textures and high T_{eq} (e.g. Harte, 1987; Witt and Seck, 1987). The interpretation for this enrichment usually invokes emplacement of pyroxenite veinlets that originated from migrating basaltic melts under high melt/rock conditions (e.g. Bedini et al., 1997). Such conditions are affirmed here by the pyroxene megacrysts and clinopyroxenite xenoliths (Tables 3 and 4; Fig. 4a) that coexist with the peridotite xenoliths. Put another way, because our examples of Fe–Ti metasomatism are in the high T_{eq} and porphyroclastic xenoliths, which implies regimes of plume proximity, they can represent metasomatism by pyroxenite veinlets emplaced in stressed and deformed lithospheric mantle regimes as they passed over partially melting asthenospheric plume. There is no evidence for Fe–Ti metasomatism in the cooler protogranular xenoliths that REE patterns suggest were infiltrated by relatively evolved small percentage melts.

9. Conclusions

The main thrust of this study is that a suite of 32 spinel lherzolite and harzburgite xenoliths from seven Tertiary basaltic centers in northeastern Brazil reflect what appears to be lithosphere with a geotherm elevated over that for stable subcontinental lithosphere. We attribute the geothermal gradient recorded in the xenoliths to thermal perturbation from the Fernando de Noronha asthenospheric plume, beginning about 40 Ma, which generated the Tertiary basaltic magmas that entrained the xenoliths ~30–13 Ma. According to the equilibration temperatures of ~800–1250 °C that represent the entire spinel peridotite stability field, the geotherm was ~12 °C/km.

The geotherm overprints subcontinental lithosphere that had a pre-Tertiary melting history. Varying degrees of partial melting in the subcontinental lithosphere can be attributed to events as recent as the Mesozoic magmatism associated with the breakup of the equatorial Atlantic region beginning ~200 Ma.

Two kinds of metasomatic processes were part of that plume-impacted lithosphere. The porphyroclastic xenoliths, with highest equilibration temperatures (>1200 °C) are associated with Fe–Ti metasomatism and modest LREE/HREE ratios. Pyroxene megacrysts and clinopyroxenite coexisting with the peridotite suite may be the modal expressions of that Fe–Ti metasomatism, as they probably represent veins emplaced in subcontinental lithosphere as basaltic melts from the Fernando de Noronha plume during Tertiary magmatism. The protogranular xenoliths, with

$T_{eq} < 1200$ °C, have notable LREE/HREE ratios that imply highly incompatible element metasomatism. This metasomatism probably also originated with plume-related fluids but more strongly reflects chromatographic effects.

Acknowledgements

This work is supported in part by NSF grant OCE8509894 (RF). We are grateful to personnel at the Oregon State University radiation center for providing instrumental neutron activation analyses for several trace elements under the US Department of Energy reactor sharing grant. We acknowledge constructive critiques by E. Piccirillo, W. Griffin, G. Kurat, C. Neal, and C. Stern.

References

Affaton, P., Rahaman, M.A., Trompette, R., Sougy, J., 1991. The Dahomeyide Orogen: tectonothermal evolution and relationships with the Volta Basin. In: Dallmeyer, R.D., Lecorche, J.P. (Eds.). The West African Orogens and Circum-Atlantic Correlatives. Springer, Berlin, pp. 107–122.

Ballhaus, C., Berry, R.G., Green, D.H., 1991. High pressure experimental calibration of the olivine-orthopryoxene-spinel oxygen geobarometer: implications for the oxidiation state of the upper mantle. Contrib. Mineral Petrol. 109, 27–40.

Batanova, V.G., Sopbolev, A.V., 2000. Compositional heterogeniety in subduction related mantle peridodite, Troodos massif, Cypress. Geology 28, 55–58.

Bedini, R.M., Bodinier, J.L., Duatria, J.M., Morten, L., 1997. Evolution of LILE-enriched small melt fractions in the lithospheric mantle: a case study from the East African Rift. Earth Planet Sci. Lett. 153, 67–83.

Bellieni, G., Macedo, M., Petrini, R., Piccirillo, E.M., Cavazzini, G., Comin-Chiaramonti, P., Ernesto, M., Macedo, J., Martins, G., Melfi, A.J., Pacca, I.G., DeMin, A., 1992. Evidence for magmatic activity related to middle Jurassic and lower Cretaceous rifting from northeastern Brazil (Ceará–Mirim): K/Ar age, paleomagnetism, petrology, and Sr–Nd isotope characteristics. Chem. Geol. 97, 9–32.

Bodinier, J.L., Vasseur, G., Vernieres, J., Dupuy, C., Fabries, J., 1990. Mechanism of mantle metasomatism: geochemcal evidence from the Lherz orogenic peridotite. J. Petrol. 31, 597–628.

Brey, G.P., Kohler, T., 1990. Geothermobarometry in four-phase lherzolite II. New thermobarometers, and practical assessment of existing thermobarometers. J. Petrol. 31, 1353–1378.

Castro, D.L., Barbosa, C.C.F., Silva, J.B.C., Medeiros, W.E., 1997a. Relevo da interface crossta-manto no Nordeste setentrional do Brasil: comparacao entre vinculos de isostasia e suavidade. Fifth Congr. Int. Soc. Bras. Geofisica, São Paulo, Abs. 2, 682–685.

Castro, D.L., Medeiros, W.E., Moreira, J.A., Jardim de Sa, E.F., 1997b. Mapa gravimetrico do Nordeste setentrional do Brasil e margem continental adjacente. Fifth Congr. Int. Soc. Bras. Geofisica, São Paulo, Abs. 2, 678–681.

Chapman, D.S., 1986. Thermal gradients in the continental crust. In: Dawson, J.B., Carswell, D.A., Hall, J., Wedepohl, K.H. (Eds.). The Nature of the Lower Continental Crust. Geological Society Special Publication, vol. 24. Blackwell, London, pp. 63–70.

Comin-Chiaramonti, P., Demarchi, G., Girardi, V.A., Princivalle, F., Sinigoi, S., 1986. Evidence of mantle metasomatism and heterogeneity from peridotite inclusions on northeastern Brazil and Paraguay. Earth Planet. Sci. Lett. 77, 203–217.

Dallmeyer, R.D., Lecorche, J.P., 1991. The West African Orogens and Circum-Atlantic Correlatives. Springer, Berlin 405 p.

Darros de Matos, R.M., 1992. The northeast Brazilian rift system. Tectonics 11, 766–791.

Downes, H., 1990. Shear zones in the upper mantle—relation between geochemical enrichment and deformation in mantle peridotites. Geology 18, 337–374.

Fan, Q., Hooper, P.R., 1989. The mineral chemistry of ultramafic xenoliths of eastern China: implications for upper mantle composition and the paleogeotherms. J. Petrol. 30, 1117–1158.

Fodor, R.V., Sial, A.N., Mukasa, S.B., McKee, E.H., 1990. Petrology, isotope characteristics, and K–Ar ages of the Maranhão, northern Brazil, Mesozoic basalt province. Contrib. Mineral. Petrol. 104, 555–567.

Fodor, R.V., Mukasa, S.B., Sial, A.N., 1998. Isotopic and trace-element indications of lithospheric and asthenospheric components in Tertiary alkalic basalts, northeastern Brazil. Lithos 43, 197–217.

Franz, L., Seifert, W., Kramer, W., 1997. Thermal evolution of the mantle underneath the Mid-German crystalline rise: evidence from mantle xenoliths from the Rhön area (Central Germany). Mineral. Petrol. 61, 1–25.

Godard, M., Bodinier, J.L., Vasseur, G., 1995. Effects of mineralogical reactions on trace element redistribution in mantle rocks during percolation processes: a chromatographic approach. Earth Planet. Sci. Lett. 133, 449–461.

Harte, B., 1987. Metasomatic events recorded in mantle xenoliths: an overview. In: Harte, B. (Ed.). Mantle Xenoliths. Wiley, New York, pp. 625–640.

Irving, A.J., Frey, F.A., 1984. Trace-element abundances in megacrysts and their host basalts: constraints on partition coefficients and magacryst genesis. Geochim. Cosmochim. Acta 48, 1201–1222.

Klemme, S., O'Neill, H.S., 2000. The near-solidus transition from garnet lherzolite to spinel lherzolite. Contrib. Mineral. Petrol. 138, 237–248.

Köhler, T.P., Brey, G.P., 1990. Calcium exchange between olivine and clinopyroxene calibrated as a geothermobarometer for natural peridotites from 2 to 60 kb with applications. Geochem. Cosmochim. Acta 54, 2375–2388.

Leitch, A.M., Davies, G.F., Wells, M., 1998. A plume head melting under a rifting margin. Earth Planet Sci. Lett. 161, 161–177.

Marzoli, A., Renne, P.R., Piccirillo, E., Ernesto, M., Bellieni, G., DeMin, A., 1999. Extensive 200 million year old continental flood basalts of the Central Atlantic Magmatic Province. Science 284, 616–618.

Mercier, J.C., Nicolas, A., 1975. Textures and fabrics of upper mantle peridotites as illustrated by basalt xenoliths. J. Petrol. 16, 454–487.

Morgan, W.J., 1983. Hot spot tracks and the early rifting of the Atlantic. Tectonophysics 94, 123–139.

Navon, O., Stolper, E., 1987. Geochemical consequence of melt percolation: the upper mantle as a chromatigraphic column. J. Geol. 95, 285–307.

Nurnberg, D., Muller, R.D., 1991. The tectonic evolution of the South Atlantic from Late Jurassic to present. Tectonophysics 191, 27–53.

O'Connor, J.M., Duncan, R.A., 1990. Evolution of the Walvis Ridge–Rio Grande rise hot spot system: implications for African and South American plate motions over plumes. J. Geophys. Res. 95, 17475–17502.

O'Neill, H.S., 1981. The transition between spinel lherzolite and garnet lherzolite, and its use as a geobarometer. Contrib. Mineral. Petrol. 77, 185–194.

O'Reilly, S.Y., Griffin, W.L., 1996. 4-D lithosphere mapping: methodology and examples. Tectonophysics 262, 3–18.

O'Reilly, S.Y., Chen, D., Griffin, W.L., Ryan, C.G., 1997. Minor elements in olivine from spinel lherzolite xenoliths: implications for thermobarometry. Mineral. Magazine 61, 257–269.

Pike, M.E., Schwarzman, E.C., 1977. Classification of textures in ultramafic xenoliths. J. Geol. 85, 49–62.

Princivalle, F., Salviulo, G., Fabro, C., Demarchi, G., 1994. Inter- and intracrystalline temperature and pressure estimates on pyroxenes from northeast Brazil mantle xenoliths. Contrib. Mineral. Petrol. 116, 1–6.

Rabinowitz, P.D., LaBreque, J., 1979. The Mesozoic South Atlantic Ocean

and evolution of its continental margins. J. Geophys. Res. 84, 5973–6002.

Righter, K., Carmichael, I.S., 1993. Mega-xenocrysts in alkalic olivine basalts: fragments of disrupted mantle assemblages. Am. Mineral. 78, 1230–1245.

Rivalenti, G., Mazzucchelli, M., Girardi, V.A., Vannucci, R., Barbieri, M.A., Zanetti, A., Goldstein, S.L., 2000. Composition and processes of the mantle lithosphere in northeastern Brazil and Fernando de Noronha: evidence from mantle xenoliths. Contrib. Mineral. Petrol. 138, 308–325.

Shaw, C.S., Eyzaguirre, J., 2000. Origins of megacrysts in the mafic alkaline lavas of the West Eifel volcanic field. Germany Lithos 50, 75–90.

Sial, A.N., 1977. Petrology and mineral chemistry of peridotite nodules included in Tertiary basaltic rocks of northeast Brazil. Geol. Soc. Am. Bull. 88, 1173–1176.

Song, Y., Frey, F.A., 1989. Geochemistry of peridotite xenoliths in basalt from Hannuoba, eastern China: implications for subcontinental mantle hetrogeniety. Geochim, Cosmoschim. Acta 53, 97–114.

Vernieres, J., Godard, M., Bodinier, J.L., 1997. A plate model for the simulation of trace element fractionatio during partial melting and magma transport in the earth's upper mantle. J. Geophys. Res. 102, 24771–24784.

Webb, S.A., Wood, B.J., 1986. Spinel-pyroxene-garnet relationships and their dependencies on Cr/Al ratios. Contrib. Mineral. Petrol. 92, 471–480.

Wells, P.R.A., 1977. Pyroxene thermometry in simple and complex systems. Contrib. Mineral. Petrol. 62, 129–139.

Wilshire, H.G., Shervais, J.W., 1975. Al-augite and Cr-diopside ultramafic xenoliths in basaltic rocks from western United States: structural and textural relationships. Phys. Chem. Earth 9, 257–272.

Wilson, M., 1997. Thermal evolution of the Central Atlantic passive margin: continental break-up above a Mesozoic super-plume. Geol. Soc. Lond 154, 491–495.

Witt, G., Seck, H.A., 1987. Temperature history of sheared mantle xenoliths from the West Eifel, West Germany: evidence for mantle diapirism beneath the Rhenish Massif. J. Petrol. 28, 475–493.

Witt-Eickschen, G., Seck, H.A., Reys, C., 1993. Multiple enrichment processes and their relationships in the subcrustal lithosphere beneath the Eifel (Germany). J. Petrol. 34, 1–22.

Xu, S., O'Reilly, S.Y., Griffin, W.L., Zhou, X., 1996. A xenolith-derived geotherm and the crust-mantle boundary at Qilin, southeast China. Lithos 38, 41–62.

Xu, Y.G., Menzies, M.A., Bodinier, J.L., Bedini, R.M., Vroon, P., Mercier, J.C., 1998. Melt percolation and reaction atop a plume: evidence from the poikiloblastic peridotite xenoliths from Borée (Massif Central, France). Contrib. Mineral. Petrol. 132, 65–84.

Zangana, N.A., Downes, H., Thirlwall, M.G., Hegner, E., 1997. Relationship between deformation, equilibration temperatures, REE and radiogenic isotopes in mantle xenoliths (Ray Pic, Massif Central, France): an example of plume-lithosphere interaction?. Contrib. Mineral. Petrol. 127, 187–203.

Zangana, N.A., Downes, H., Thirlwall, M.G., Marriner, G.F., Bea, F., 1999. Geochemical variation in peridotite xenoliths and their constituent clinopyroxenes from Ray Pic (French Massif Central): implications for the composition of the shallow lithospheric mantle. Chem. Geol. 153, 11–35.